3 Performance enhancement techniques for indoor VLC systems

Wen-De Zhong and Zixiong Wang

3.1 Introduction

Light-emitting diodes (LEDs) have been widely deployed for illumination, due to their high performance and energy efficiency properties compared with conventional incandescent and fluorescent lamps [1]. In addition, advantages such as high frequency response, free spectrum license and high security have made LEDs a promising means for wireless communications, whereby people can access the internet through the same visible light. Significant research has been carried out to develop indoor high data rate visible light communication (VLC) systems [1–11]. The data rate of VLC systems in a laboratory environment has been demonstrated to reach the order of Gb/s [12, 13]. In addition, advanced modulation schemes such as spatial modulation [14–17] have been introduced to VLC systems to enhance the data rate considerably. In 2011, light-fidelity (Li-Fi) was introduced by Haas [18], who demonstrated that a VLC system can be leveraged to develop an alternative method of accessing network resources as a substitute for wireless fidelity (Wi-Fi). Although there has been significant progress in this area in the past decade, there are still some challenges to overcome in order to implement and deploy VLC systems [19] on a larger scale. Two major challenges are selection of an uplink transmission approach, and design of energy-saving receivers for long transmission distance. In this chapter, a number of recently proposed techniques [20–25] for enhancing the performance of indoor VLC systems are discussed along with results pertaining to their performance. These include a receiver plane tilting technique [21] and an LED lamp arrangement approach [22, 23] to improve the signal-to-noise ratio (SNR) and bit error rate (BER) performances, and performance evaluation of VLC systems under a dimming control scheme [20, 24].

3.2 Performance improvement of VLC systems by tilting the receiver plane

In a VLC system, the receiver may be located far from the LED lamp, where the SNR is much smaller than at those locations that are close to the lamp. The lower SNR is obtained as the distance from the source increases and as the incident angle increases. This section describes a receiver plane tilting technique [21] to improve the

performance of the VLC system across the entire room. The dimension of the room is assumed to be 5 m length × 5 m width × 3 m height. The SNRs with/without tilting the receiver plane are analyzed and compared. For simplicity, the reflections of walls are not considered in analyzing the SNR since the light from the line-of-sight (LOS) is dominant.

3.2.1 SNR analysis of VLC system with a single LED lamp

Figure 3.1 illustrates the geometry of an indoor VLC system with one LED lamp located on the ceiling. The parameters of the VLC system considered in this chapter are given in Table 3.1. The LED lamp is assumed to be located at the center of the ceiling whose position is [2.5 m, 2.5 m, 3.0 m], and the photo-detector (receiver) is on a desk with a height of 0.85 m from the floor. Let φ be the angle of radiation with respect to the axis normal to the LED surface (plane). Following [1, 8], the emitted light from an LED is assumed to have a Lambertian emission pattern, and the radiation pattern is given by:

$$R(\varphi) = \frac{(m+1)\cos^m\varphi}{2\pi}, \tag{3.1}$$

where m is the order of Lambertian emission, which is related to the transmitter's semi-angle at half power $\varphi_{1/2}$ as $m = \ln(1/2)/\ln(\cos\varphi_{1/2})$.

The frequency response of the LED and photo-detector is assumed to be flat within the modulation bandwidth of the signals considered in this chapter. Considering only the LOS transmission path, the channel DC gain is given by [1, 27]

$$H(0) = R(\varphi)\frac{A}{d^2}\cos\theta = \frac{(m+1)\cos^m\varphi A}{2\pi d^2}\cos\theta, \tag{3.2}$$

where d is the distance between the LED source and the receiver, A is the physical area of photo-detector, and θ is the angle of incidence with respect to the axis normal to the desk

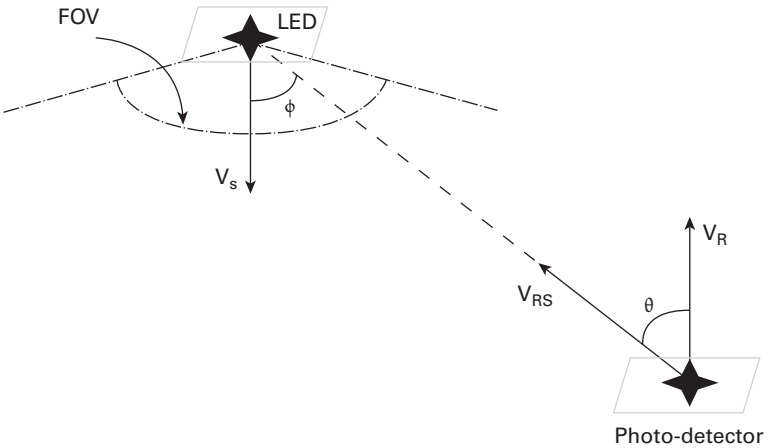

Figure 3.1 Geometry of the LED source and photo-detector (receiver) in the VLC system.

Table 3.1 Parameters of the VLC system considered in this chapter [1, 20–22].

Room size (length × width × height)	5 m × 5 m × 3 m
Height of desk where the receiver is located	0.85 m
Transmitter's semi-angle at half power ($\varphi_{1/2}$)	60 °
Physical area of photo-detector (A)	10^{-4} m^2
Receiver's field of view (FOV)	170 °
Responsivity of photo-detector (R)	1 A/W
Background current (I_{bg})	5100 μA
Noise bandwidth factor (I_2)	0.562
Field-effect transistor (FET) transconductance (g_m)	30 mS
FET channel noise factor (Γ)	1.5
Fixed capacitance (η)	112 pF/cm^2
Open-loop voltage gain (G)	10
Definite integral involved in expression of circuit noise (I_3) [26]	0.0868

plane where the LED is located. Angles φ and θ are associated with the locations/positions of both LED source and receiver. Let $[X_S, Y_S, Z_S]$ and $[X_R, Y_R, Z_R]$ be the locations (coordinates) of source and receiver, respectively. With reference to Fig. 3.1, the radiation angle φ is determined by

$$\cos\varphi = \frac{Z_S - Z_R}{\|[X_S, Y_S, Z_S] - [X_R, Y_R, Z_R]\|}, \tag{3.3}$$

where $\|X\|$ is the norm of X. Equation (3.3) indicates that the radiation angle φ is constant for the given locations of the source and receiver. The value of the incident angle θ is determined not only by the locations of source and receiver, but also by the dihedral angle between the receiver plane and the desk plane where the receiver is located. With reference to Fig. 3.1, let $\boldsymbol{v_{RS}}$ be the vector from the receiver to the source, and $\boldsymbol{v_R}$ be the vector of the receiver. Then the incident angle θ is calculated by

$$\cos\theta = \frac{(\boldsymbol{v_R}, \boldsymbol{v_{RS}})}{\|\boldsymbol{v_R}\| \cdot \|\boldsymbol{v_{RS}}\|}, \tag{3.4}$$

where $(\boldsymbol{v_{RS}}, \boldsymbol{v_R})$ is the inner product of $\boldsymbol{v_{RS}}$ and $\boldsymbol{v_R}$. Substituting Eq. (3.4) into Eq. (3.1), the channel DC gain in Eq. (3.1) becomes [21]

$$H(0) = \frac{(m+1)}{2\pi d^2} \mathrm{A} \cos^m\varphi \frac{(\boldsymbol{v_R}, \boldsymbol{v_{RS}})}{\|\boldsymbol{v_R}\| \cdot \|\boldsymbol{v_{RS}}\|}. \tag{3.5}$$

Assume that the LED light is modulated with a modulating signal $f(t)$. The optical signal at the output of an LED can be expressed by $p(t) = P_t\,(1 + M_I\,f(t))$, where P_t is the launched power of the LED lamp and M_I is the modulation index [28], which is assumed to be 0.2. The received optical power P_r is given by

$$P_r = H(0)P_t. \tag{3.6}$$

After photo-detection and considering that the DC component of the detected signal is filtered out in the receiver, the output electrical signal is given by

$$s(t) = RP_r M_I f(t), \tag{3.7}$$

where R is the responsivity of the photo-detector. Hence, the SNR of the output electrical signal can be calculated by [5],

$$SNR = \frac{\overline{s(t)^2}}{P_{\text{noise}}} = \frac{(RH(0)P_t M_I)^2 \overline{f(t)^2}}{P_{\text{noise}}}, \tag{3.8}$$

where $\overline{s(t)^2}$ is the average power of the output electrical signal, and P_{noise} is the noise power. The noise power consists of both shot noise and thermal noise, whose variances are given by [1],

$$\sigma_{\text{shot}}^2 = 2q\left[RP_r\left(1 + \overline{\left(M_{\text{index}} f(t)\right)^2}\right) + I_{\text{bg}} I_2\right]B, \tag{3.9}$$

$$\sigma_{\text{thermal}}^2 = 8\pi k T_{\text{K}} \eta A B^2 \left(\frac{I_2}{G} + \frac{2\pi\Gamma}{g_{\text{m}}} \eta A I_3 B\right), \tag{3.10}$$

where $P_r\left(1 + \overline{\left(M_{\text{index}} f(t)\right)^2}\right)$ is the total received power, q is the electron charge [13], B is the equivalent noise bandwidth, k denotes the Boltzmann constant, and T_{K} represents the absolute temperature. The parameters in Eqs. (3.1)–(3.10) and other parameters used in the VLC system are listed in Table 3.1.

Using Eq. (3.8), the SNR distribution of the receiver located on the desk plane at the height of 0.85 m can be calculated. In calculating the SNR distribution, the parameters in Table 3.1 are used. Figure 3.2 shows the SNR distribution for the case when the launching power of the LED lamp is 5 W, and the LED is located at the center of the ceiling. As shown in Fig. 3.2, the maximum SNR is 28.94 dB when the receiver is located right below the LED, while the minimum SNR is 6.23 dB when the receiver is placed at a corner of the room. Thus, the peak-to-trough SNR difference is 22.70 dB. Note that the SNR vertical tint bar on the right hand side of the figure indicates the relationship between the SNR value and the color (black represents the smallest value of SNR; while white denotes the highest value of SNR). The large variation of the SNR in a room can significantly reduce the overall system performance [21]. The large SNR difference in a room is caused not only by the distance between the LED and the receiver, but also by the non-normal incidence of the light from the LED to the receiver. For the given locations of the LED and receiver, the distance between the LED and the receiver cannot be changed. However, the incident angle of the light from the LED to the receiver can be adjusted to reduce the SNR variation.

3.2.2 Receiver plane tilting technique to reduce SNR variation

As described above, the non-normal incidence of the light could result in a large SNR variation in a room. The incident angle θ is determined by the vectors $\boldsymbol{v_R}$ and $\boldsymbol{v_{RS}}$. Note that the vector $\boldsymbol{v_R}$ is always perpendicular to the receiver plane. The vector $\boldsymbol{v_{RS}}$ is constant for

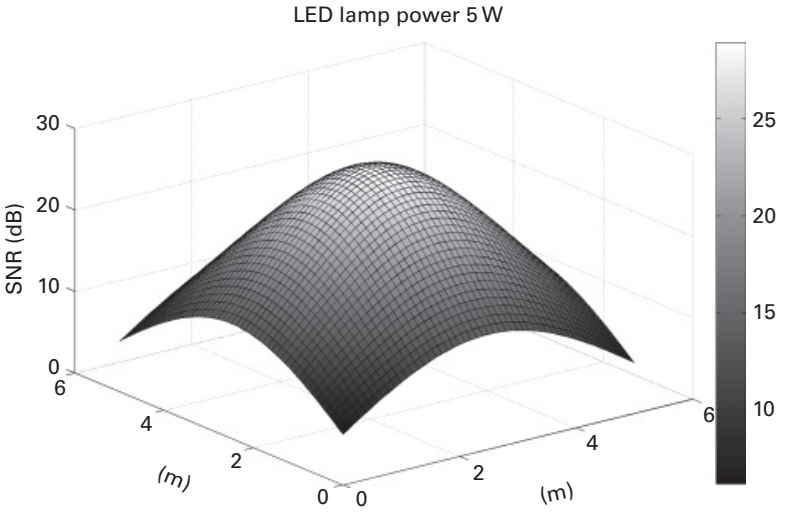

Figure 3.2 SNR distribution of VLC system in a room with one LED lamp located on the center of the ceiling.

the given locations of the source and receiver. According to Eq. (3.4), $\cos\theta$ reaches its maximum when the two vectors $\boldsymbol{v_{RS}}$ and $\boldsymbol{v_R}$ are parallel to each other, i.e., the receiver plane faces the source. In the case where the receiver is not located on the desk right below the source on the ceiling, especially when the receiver is positioned in one of the corners of the room, the maximum channel DC gain is greatly reduced as the incident angle θ increases. However, by tilting the receiver plane towards the source such that the two vectors $\boldsymbol{v_{RS}}$ and $\boldsymbol{v_R}$ become parallel to each other, the value of $\cos\theta$ reaches its maximum and thus maximum channel DC gain of a particular position can be attained, which is only associated with the transmission distance d and the angle of radiation φ [21].

Vector $\boldsymbol{v_{RS}}$ can be expressed as $\boldsymbol{v_{RS}} = [a, b, c] = [X_R, Y_R, Z_R] - [X_S, Y_S, Z_S]$. Here we assume that tilting the receiver plane does not change the position of the receiver. In the spherical coordinate system, the location of the receiver is selected as the origin. Before tilting the receiver plane, the vector $\boldsymbol{V_R}$ is [0, 0, 1], which means that the receiver plane points to the ceiling. After tilting the receiver plane towards the LED source on the ceiling, the vector $\boldsymbol{V_R}$ becomes $[\sin\beta\cdot\cos\alpha, \sin\beta\cdot\sin\alpha, \cos\beta]$, where β is the inclination angle [29] which is equal to the tilting angle, as shown in Fig. 3.3 and the azimuth angle α is determined by the positions of the receiver as well as the source projection on the desk. In the Cartesian coordinate system with the receiver as the origin, the value of angle α is given by Eq. (3.11):

$$\alpha = \begin{cases} \arctan\left(|(Y_S - Y_R)/(X_S - X_R)|\right) & \text{source projection in the 1st quadrant,} \\ \pi - \arctan\left(|(Y_S - Y_R)/(X_S - X_R)|\right) & \text{source projection in the 2nd quadrant,} \\ \pi + \arctan\left(|(Y_S - Y_R)/(X_S - X_R)|\right) & \text{source projection in the 3rd quadrant,} \\ 2\pi - \arctan\left(|(Y_S - Y_R)/(X_S - X_R)|\right) & \text{source projection in the 4th quadrant.} \end{cases} \tag{3.11}$$

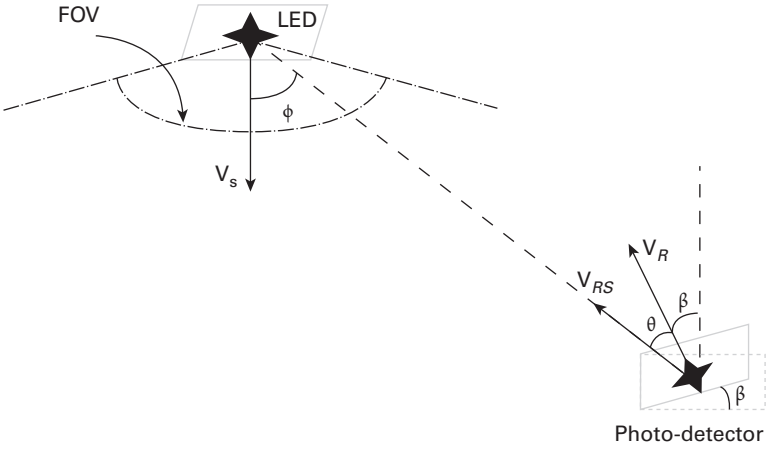

Figure 3.3 Geometry of the LED source and photo-detector after tilting the receiver plane.

Thus, $\cos\theta$ in Eq. (3.4) becomes

$$\cos\theta = \frac{(\boldsymbol{v_R}, \boldsymbol{v_{RS}})}{\|\boldsymbol{v_R}\| \cdot \|\boldsymbol{v_{RS}}\|} = \frac{a\sin\beta\cos\alpha + b\sin\beta\sin\alpha + c\cos\beta}{\sqrt{a^2+b^2+c^2}}. \tag{3.12}$$

Substituting Eq. (3.12) into Eq. (3.5), the channel DC gain after tilting the receiver plane, denoted by $f(\beta)$, becomes,

$$f(\beta) = \frac{(m+1)\cos^m\varphi A}{2\pi d^2\sqrt{a^2+b^2+c^2}}(a\sin\beta\cos\alpha + b\sin\beta\sin\alpha + c\cos\beta). \tag{3.13}$$

Since the receiver is located on the desk, the initial inclination angle β is zero. This receiver plane tilting technique can be implemented by electrical machinery. When the inclination angle is increased after tilting the receiver plane, the two vectors $\boldsymbol{v_R}$ and $\boldsymbol{v_{RS}}$ tend to become parallel to each other and thereby the received optical power increases. The electrical machinery will not stop changing the inclination angle β until the received optical power does not increase any more.

The Newton method (a fast algorithm to find the maximum value of $f(\beta)$ [30]) can be employed to search for the optimum inclination angle β. After finding the optimum tilting angle by the Newton method, the maximum optical power is obtained for each receiver position. Figure 3.4 shows the improved SNR distribution. The maximum SNR remains unchanged at 28.94 dB, while the minimum SNR at each corner of the room is increased to 11.92 dB, resulting in an improvement of 5.69 dB in the peak-to-trough SNR difference as compared to the case without tilting the receiver plane.

3.2.3 Multiple LED lamps with the receiver plane tilting technique

To further reduce the SNR variation, multiple LED lamps could be employed in conjunction with the receiver plane tilting technique [21]. As an example, consider a case where four LED lamps are located on the ceiling at the positions of [1.5 m, 1.5 m,

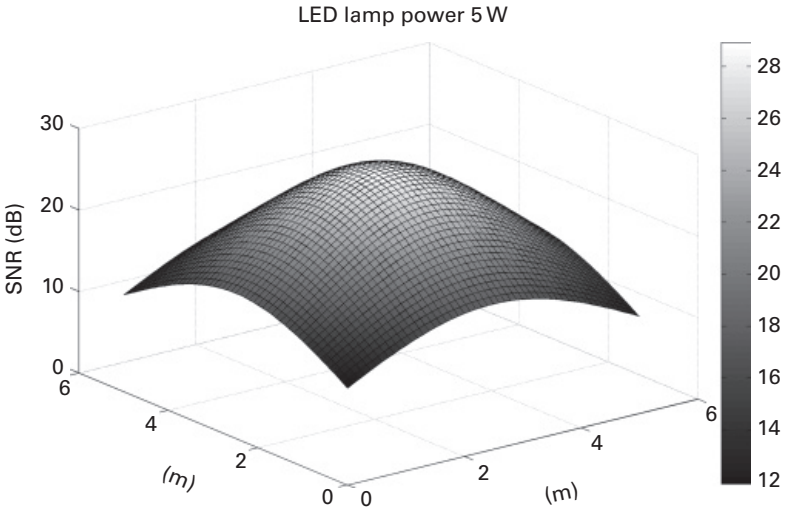

Figure 3.4 SNR distribution of VLC system in a room with one LED lamp on the center of the ceiling after tilting the receiver plane.

3.0 m], [1.5 m, 3.5 m, 3.0 m], [3.5 m, 1.5 m, 3.0 m] and [3.5 m, 3.5 m, 3.0 m], respectively. As the light is received from all of the four LED lamps, the channel DC gain in Eq. (3.2) is modified as follows:

$$H(0) = \sum_{i=1}^{4} \frac{(m+1)A\cos^m\varphi_i}{2\pi d_i^2}\cos\theta_i, \tag{3.14}$$

where the subscript i denotes lamp i. In this case, the total radiating power from the four LEDs remains unchanged at 5 W, i.e., the launching power of each LED lamp is reduced to one quarter of that of one LED lamp in subsection 3.2.2. Figure 3.5 (a) shows the SNR distribution with four LED lamps without tilting the receiver plane. As shown in Fig. 3.5 (a), the maximum and minimum SNRs are 22.72 dB and 8.95 dB, respectively. That is, the peak-to-trough SNR difference is 13.77 dB without tilting the receiver plane. It is also observed that in the area inside the projections of the LEDs on the desk plane, the SNR distribution is almost constant and hence there is no need to adjust the SNR distribution within this area [21].

However, the SNR variation is quite large in the places outside projections of the four LEDs on the desk plane. In such places, the SNR difference can be reduced by tilting the receiver plane in the same way as described for the case of a single LED lamp.

When the receiver is not equidistant with respect to any of two LEDs, it faces the nearest LED of the four, which determines the value of azimuth angle α. When the receiver is equidistant from two LEDs, it faces to the middle of them. The total channel DC gain after tilting the receiver plane, denoted as $f(\beta)$, is given by

$$f(\beta) = \frac{(m+1)A\cos^m\varphi}{2\pi d^2\sqrt{a^2+b^2+c^2}}(a\sin\beta\cos\alpha + b\sin\beta\sin\alpha + c\cos\beta). \tag{3.15}$$

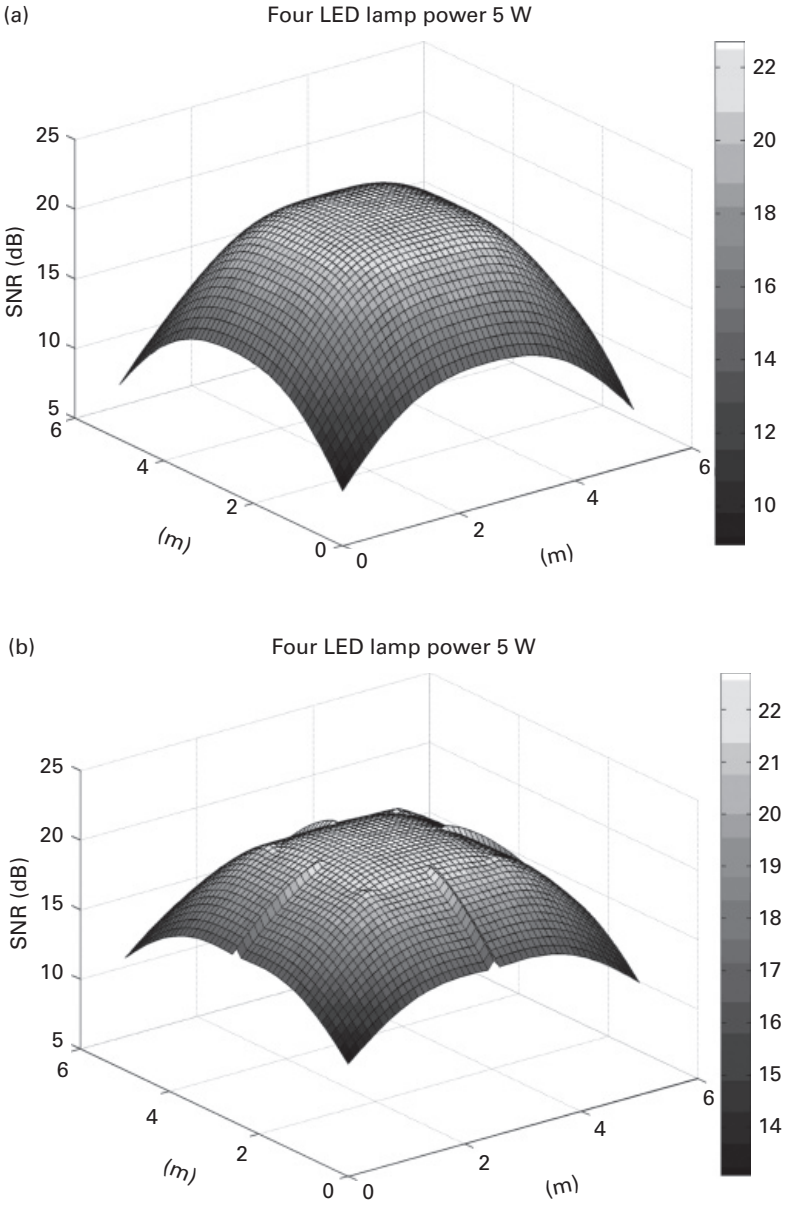

Figure 3.5 SNR distribution of VLC system in a room with four LED lamps located on the ceiling: (a) before; and (b) after tilting the receiver plane (after [21]).

As in the case of a single LED lamp, the optimum tilting angle β can then be obtained by the Newton method. Figure 3.5 (b) shows the improved SNR distribution with the receiver tilting technique. As shown in Fig. 3.5 (b), the maximum SNR remains at 22.72 dB, while the minimum SNR increases to 13.09 dB. That is, the peak-to-trough SNR difference is reduced from 13.77 dB to 9.63 dB. In other words, a 4.14 dB

improvement in the peak-to-trough SNR difference is achieved. In the case of four LED lamps, the study shows that only three search steps are required by the Newton algorithm to converge to the optimum value [21].

3.2.4 Spectral efficiency

Tilting the receiver plane makes it possible to attain optimum SNR. A higher SNR per symbol (E_s/N_0) means a better bit error rate (BER) performance. As discussed above, the SNR can vary considerably within the room. Similarly to RF wireless communications, adaptive advanced modulation formats such as M-ary quadrature amplitude modulation (M-QAM) orthogonal frequency division multiplexing (OFDM) can be employed to enhance transmission capacity [31]. This subsection discusses the spectral efficiency of a single user VLC system employing adaptive M-QAM OFDM. Figure 3.6 is a block diagram for a VLC system with adaptive M-QAM OFDM, where the value of M represents the number of points in the signal constellation and can be varied in accordance with the SNR. Here it is assumed that infrared (IR) or another kind of wireless technology is employed to provide channel feedback as well as uplink transmission.

Following [32, 33] and applying gray coding for the mapping of the M-QAM signal, the BER of the M-QAM OFDM signal is given by

$$\mathrm{BER} \approx \frac{4}{\log_2(M)}\left(1-\frac{1}{\sqrt{M}}\right) Q\left(\sqrt{\frac{3\log_2(M)}{M-1}\frac{E_b}{N_0}}\right), \tag{3.16}$$

where $Q(\cdot)$ is the Q-function. Note that the relationship between SNR per symbol (E_s/N_0) and SNR per bit (E_b/N_0) is given by $E_s/N_0 = \log_2(M) \times E_b/N_0$ [33].

As shown in Fig. 3.6, when the M-QAM OFDM optical signal reaches the photodetector, its power is detected and sent back to the sources on the ceiling via the IR feedback channel after tilting the receiver plane. Here the benchmark BER is set at 10^{-3}, which satisfies the requirement of error-free transmission by applying a forward-error correction (FEC) code [34]. A smaller value of M should be chosen to attain a BER of 10^{-3} at the locations/positions with low SNR. However, at the places with high SNR, a larger value of M is selected to achieve a higher data rate while maintaining a steady BER of 10^{-3}. It is noted that the value of the M-QAM OFDM signal should be real in optical transmission (this is attained by applying Hermitian symmetry [4]), resulting in a 50% reduction in spectral efficiency [35, 36]. Using Eq. (3.16), the SNR per symbol threshold for achieving a BER of 10^{-3} can be calculated for a given value of M, as shown in Table 3.2, where the symbol rate is 50 Msymbol/s.

Let N be the number of subcarriers used in OFDM. Assuming that the pulse shape is rectangular, the spectral efficiency (SE) in units of bit/s/Hz of an M-QAM OFDM signal can be expressed as [37]

$$SE = \frac{1}{2}\log_2(M)\frac{N}{N+1} \approx \frac{1}{2}\log_2(M), \tag{3.17}$$

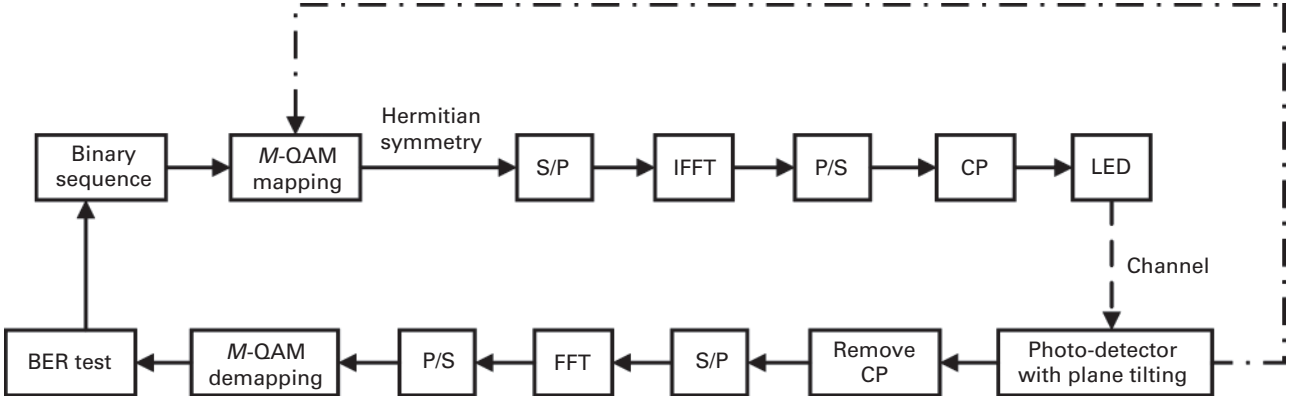

Figure 3.6 Block diagram of a VLC system employing adaptive *M*-QAM OFDM. CP: cyclic prefix, P/S: parallel to serial, S/P: serial to parallel (adapted from [21]).

Table 3.2 The calculated SNR per symbol threshold for achieving a BER of 10^{-3} for different values of M in M-QAM.

Value of M in M-QAM	4	16	64	256	1024
SNR (dB) per symbol threshold	9.8	16.5	22.5	28.4	34.2

where ½ represents the SE reduction as a result of applying the Hermitian symmetry. In a single-user VLC system using adaptive M-QAM OFDM, the value of M is varied in accordance with the value of SNR. The average SE across the entire room can be expressed by

$$\overline{SE} = \frac{1}{2}\sum_i \log_2(M_i)\, p(M_i), \tag{3.18}$$

where $p(M_i)$ is the probability that M_i-QAM is used, which can be calculated based on the SNR distribution in the room.

Figure 3.7 (a) and (b) show the average SE for the cases of one LED lamp and four LED lamps, respectively. The average SE increases with the total LED power. This is because SNR is increased with the total LED power, which in turn increases the probability of employing a larger value of M in adaptive M-QAM modulation. Figure 3.7 (a) and (b) also show the average SE improvement attained by tilting the receiver plane. In the case of one LED lamp, the average improvement is about 0.36 bit/s/Hz, and the maximum improvement is 0.47 bit/s/Hz when the LED lamp power is 9 W. In the case of four LED lamps, the average improvement is 0.18 bit/s/Hz, and the maximum improvement is 0.23 bit/s/Hz when the total LED lamp power is 19 W.

3.3 Performance improvement of VLC systems by arranging LED lamps

For an indoor VLC system, equal signal quality in terms of SNR and BER across the entire room is important; this is particularly true when there are multiple users in the room. As discussed in Section 3.2, the LED lamps are usually located around the center of the ceiling (called a centered-LED lamp arrangement) in a typical room. This centered-LED lamp arrangement makes SNR vary largely from one location/position to another [1, 21], which can significantly affect the quality of the received signal across the room. Section 3.2 analyzes and discusses the performance improvement in an indoor VLC system by tilting the receiver plane. Tilting the receiver plane can reduce the SNR variation to some extent, but it may considerably increase the complexity of the receiver design. This section describes an effective LED lamp arrangement reported in [22] to significantly reduce SNR variation and hence improve BER performance of VLC systems throughout the entire room, so that multiple users can receive signals of almost equal quality, regardless of their location.

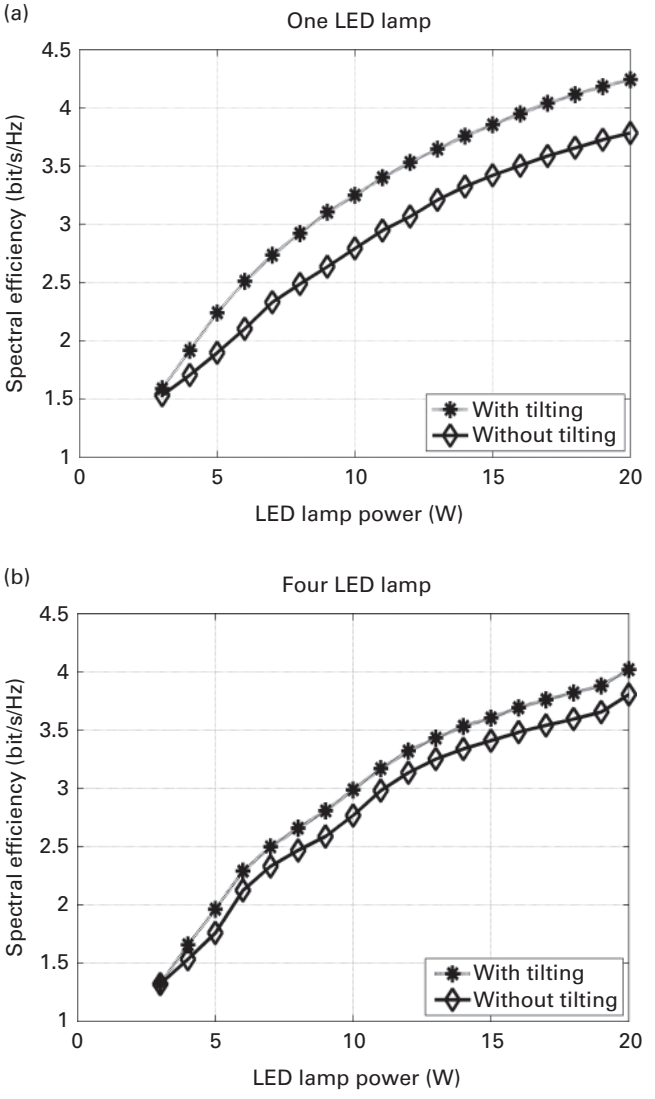

Figure 3.7 Average spectral efficiency for the cases of: (a) one LED lamp; and (b) four LED lamps, with and without tilting receiver plane (adapted from [21]).

3.3.1 Arrangement of LED lamps

In order to see the effectiveness of the LED lamp arrangement, without loss of generality, let us first consider a situation where there are 16 identical LED lamps that are located around the center of the ceiling. The interval between adjacent LED lamps is 0.2 m. Each LED lamp emits 125 mW, and hence the total power of 16 centered-LED lamps is 2 W. The other parameters of the VLC system considered here are provided in Table 3.1. 100 positions are sampled in the room. These sampled positions are uniformly distributed on

the plane where the photo-detector is located. To evaluate the quality of signal received at every location in the room, a parameter denoted Q_{SNR} is introduced, which is defined as

$$Q_{SNR} = \frac{\overline{SNR}}{2\sqrt{\text{var}(SNR)}}, \tag{3.19}$$

where $\overline{SNR}$ is the mean of SNR, and var(SNR) denotes the variance of SNR. A higher value of Q_{SNR} implies that the SNR is more uniformly distributed over the entire room. Figure 3.8 (a) illustrates the calculated SNR distribution, in which the maximum variation in SNR is about 14.5 dB. In this case, the associated Q_{SNR} is approximately 0.5 dB, which means that the SNR varies significantly throughout the room and the signal quality

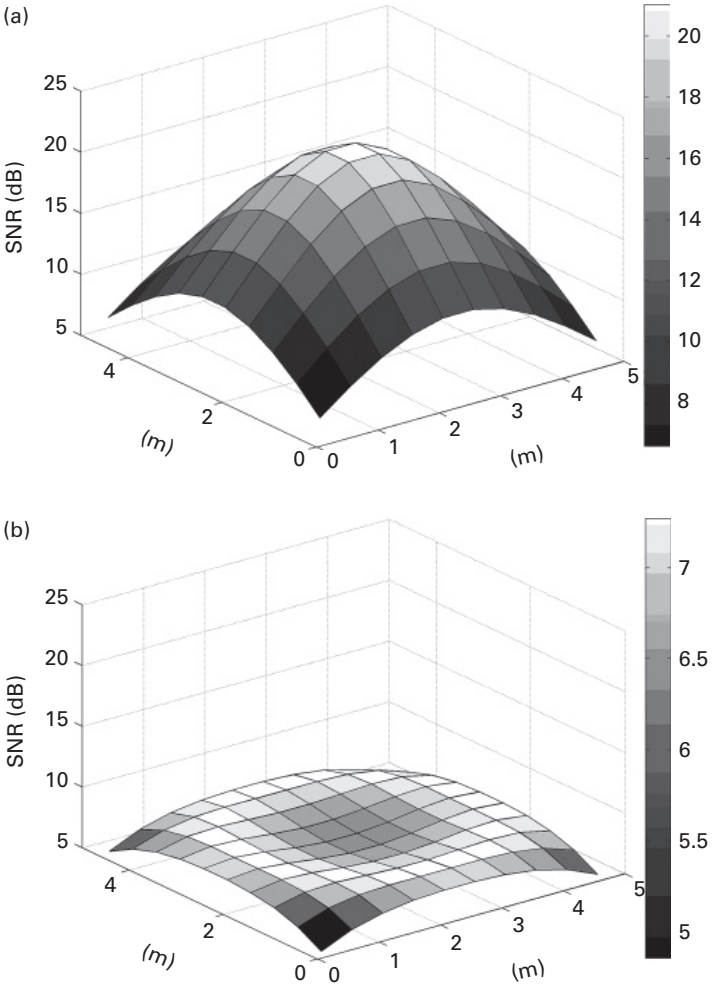

Figure 3.8 SNR distribution of a VLC system in a room with a total power of 2 W: (a) 16 centered-LED lamps; (b) 16 circle-LED lamps (adapted from [22]).

is strongly related to the user's location/position. In calculating SNR distribution, the reflections of walls or the ISI are not considered here, since the LOS light is dominant. However, they will be included in the analysis of BER performance in the next subsection.

The poor SNR distribution illustrated in Fig. 3.8 (a) arises from the centered-LED lamp arrangement, where the distances between a user in the corner of the room and the lamps are much greater than the distances between a user in the center of the room and the lamps.

If the LED lamps are located separately and symmetrically to the center of the ceiling, the SNR distribution is expected to be improved considerably, since the differences in distances between users and lamps are reduced [22]. In [22], a circle-LED lamp arrangement is proposed to reduce SNR variation. Figure 3.8 (b) shows the SNR distribution for the case of 16 lamps, where the LED lamps are distributed evenly on a circle on the ceiling with a radius of 2.5 m and each lamp emits the same amount of power as that in the case of 16 centered-LED lamps. As shown in Fig. 3.8 (b), the SNR variation is reduced largely from 14.5 dB to 2.4 dB, and the Q_{SNR} increases substantially from 0.5 dB to 9.3 dB. This demonstrates that the circle arrangement offers much better signal quality and thereby an improved communication system, which is little related to the user's position [22].

Although the Q_{SNR} is as high as 9.3 dB for the circle-LED lamp arrangement, the SNR in the four corners (which are equivalent in terms of distance) is still smaller than that in other locations, as shown in Fig. 3.8 (b). A technique to further improve the SNRs at the four corners is to add an LED lamp in each corner as described in [22]. Assume that the distances of the lamps in the corners to their nearest walls are all 0.1 m, as shown in Fig. 3.9 (a). In order to make a fair comparison, the total LED lamp power is still maintained at 2 W and the number of LED lamps placed in the circle is reduced to 12, so that the total number of LED lamps remains unchanged. Let $P_{t,\text{circle}}$ and $P_{t,\text{corner}}$ be the emitted powers of a circle-LED lamp and a corner-LED lamp, respectively. By adjusting the power of the 4 corner-LED lamps and the 12 circle-LED lamps spreading uniformly on the circle, the variance of the received optical power P_r, can be minimized, as follows [22]:

$$\min \text{var}(P_r) = \min E[(P_{r,j} - E(P_{r,j}))^2], \tag{3.20}$$

where $E(\cdot)$ denotes the mean value and $P_{r,j}$ is the received power at sampled position j, which is described by

$$P_{r,j} = \sum P_{t,\text{corner}} H(0)_{\text{corner}} + \sum P_{t,\text{circle}} H(0)_{\text{circle}}. \tag{3.21}$$

Next, the radius of the LED circle and the distance between a corner-LED and its nearest walls are changed to find the minimum SNR fluctuation. The results are given in Tables 3.3 and 3.4. As shown in Table 3.3, when the distance between the corner-LED lamps and their nearest walls is 0.1 m, the optimum radius of the LED circle is between 2.2 to 2.3 m, where Q_{SNR} is largest. Table 3.4 shows that the optimum distance between

Table 3.3 SNR and Q_{SNR} under the arrangement of 12 circle-LEDs and 4 corner-LEDs with different radii, where the distance between a corner-LED and its nearest walls is 0.1 m [22].

Radius (m)	2.1	2.2	2.3	2.5
SNR range (dB) [min, max]	[5.5, 6.4]	[5.6, 6.5]	[5.5, 6.5]	[5.3, 6.5]
Q_{SNR} (dB)	12.1	12.2	12.2	11.5

Table 3.4 SNR and Q_{SNR} under the arrangement of 12 circle-LEDs and 4 corner-LEDs with different distances between a corner-LED and its nearest walls, where the radius of the LED circle is 2.2 m [22].

Distance (m)	0.5	0.25	0.15	0.1
SNR range (dB) [min, max]	[6.0, 7.4]	[5.9, 6.8]	[5.7, 6.6]	[5.6, 6.5]
Q_{SNR} (dB)	10.7	11.7	12.1	12.2

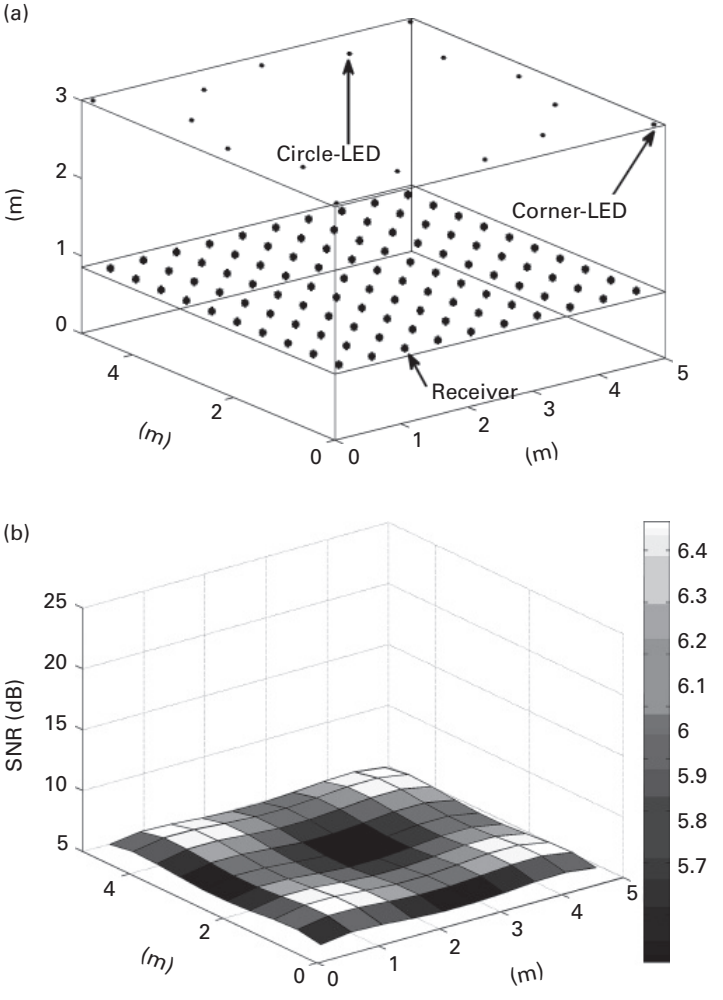

Figure 3.9 Arrangement of 12 LED lamps in a circle and 4 LED lamps in corners: (a) locations of LED lamps and 100 receivers; (b) SNR distribution with a total power of 2 W (adapted from [22]).

the corner-LED lamps and their nearest walls is 0.1 m, when the radius of the LED circle is 2.2 m. It is also found that the largest Q_{SNR} is obtained when the powers of each corner-LED lamp and each circle-LED lamp are 238 mW and 87 mW, respectively. The improved SNR distribution is shown in Fig. 3.9 (b), where the maximum SNR difference is 0.85 dB and the corresponding Q_{SNR} is 12.2 dB. The above results reveal that the arrangement of 12 circle-LED lamps and 4 corner-LED lamps with the given parameters in Table 3.1 can provide almost identical communication quality to multi-users, irrespective of their positions in the room [22].

3.3.2 BER analysis

As discussed above, the arrangement of 12 circle-LED lamps and 4 corner-LED lamps can provide almost uniformly distributed SNR to users, irrespective of their locations/positions in the room. However, this may cause an increase in ISI since the photodetector receives signals from all of the LED lamps whose distances to the receiver vary greatly, which may reduce the BER performance significantly. Without considering reflections, the maximum difference of light arrival time under the arrangement of 12 circle-LED lamps and 4 corner-LED lamps is 15.9 ns when the receiver is located in a corner position [22]; whereas the maximum time difference is only 2.34 ns when the 16 LED lamps are located in the center of the ceiling. In [22], the BER performance of both 100 Mb/s and 200 Mb/s bipolar OOK signals is analyzed and evaluated.

This subsection presents the BER analysis of a 100 Mbit/s bipolar OOK signal under the arrangement of 12 circle-LED lamps and 4 corner-LED lamps. The first order of reflection is considered in the BER analysis. Let us consider the worst case where the receiver is placed in a corner with a location of [0.25 m, 0.25 m, 0.85 m] and hence the ISI is most severe. The reflectivity and the modulation index are assumed to be 0.7 and 0.2, respectively.

Figure 3.10 (a) illustrates the pulse shape of the received bit "1" under the arrangement of 12 circle-LED lamps and 4 corner-LED lamps, as shown in Fig. 3.9 (a). As can be seen in Fig. 3.10 (a), the duration of the received bit "1" is more than 30 ns, more than three times the transmitted bit period $T = 10$ ns. Let $h = [1\ a_1 \ldots a_k]$ be the normalized channel response. It is noted that a_i ($i = 1,2,\ldots,k$) represents the ISI contribution from the present bit to the subsequent ith bit. Let I_m be the present received bit with amplitude $\pm\sqrt{E_b}$, and $I_{m-1},\ldots,I_{m-k}$ be the k preceding received bits. Considering the ISI from the k preceding bits, the present received signal y_m is expressed by

$$y_m = I_m + \sum_{i=1}^{k} a_i\, I_{m-i} + n, \tag{3.22}$$

where n is the additive white Gaussian noise (AWGN) with power spectral density of $N_0/2$. Let $P(e \mid I_m = \sqrt{E_b})$ be the conditional error probability when the present received bit is "1," i.e., amplitude is $\sqrt{E_b}$. Then $P(e \mid I_m = \sqrt{E_b})$ can be expressed by [32],

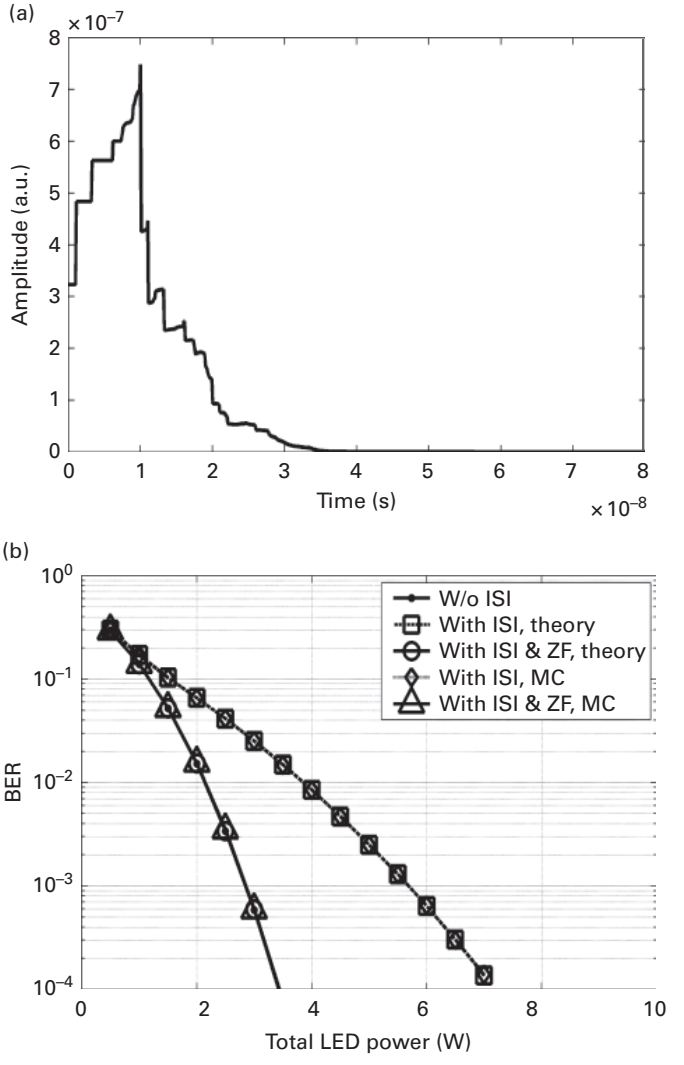

Figure 3.10 BER performance of a 100 Mbit/s bipolar OOK signal when the receiver is located at the corner: (a) the pulse shape of received bit "1" with ISI; and (b) BER with and without ZF equalization, when the total LED power is 2 W (adapted from [22]).

$$P(e\,|\,I_m=\sqrt{E_b})=\sum P(I_{m-1},\ \ldots,I_{m-k})P(e\,|\,I_m=\sqrt{E_b},\ I_{m-1},\ \ldots,I_{m-k}),\quad(3.23)$$

where $I_{m-1},\ldots,I_{m-k}$ is a combination of the k preceding received bits, and $I_{m-i}\ (i=1,\ 2,\ \ldots\ ,k)=\pm\sqrt{E_b}$, i.e., each of the k preceding received bits is either 1 or 0. Note that bit 0 is mapped to −1 for a bipolar OOK signal. $P(I_{m-1},\ldots,I_{m-k})$ is the probability of one such combination. $P(e\,|\,I_m=\sqrt{E_b},\ I_{m-1},\ \ldots,I_{m-k})$ is the conditional error probability when the present received bit is 1 and one of the

combinations of the k preceding received bits occurs. For example, when all the k preceding received bits and the present received bit are 1, the conditional error probability in Eq. (3.23) is given by

$$\begin{aligned} P(e\,|\,I_m \quad &= \sqrt{E_b},\ I_{m-1} = I_{m-2} = \ \ldots\ = I_{m-k} = \sqrt{E_b}) \\ &= P(y_m < 0\,|\,I_m = I_{m-1} = I_{m-2} = \ldots\ = \sqrt{E_b}) \\ &= P(y_m = \sqrt{E_b}\left(1 + \sum_{i=1}^{k} a_i\right) + n < 0) \\ &= P\left(n < -(1 + \sum_{i=1}^{k} a_i)\sqrt{E_b}\right) \\ &= Q\left((1 + \sum_{i=1}^{k} a_i)\sqrt{2E_b/N_0}\right), \end{aligned} \tag{3.24}$$

where $Q(\cdot)$ is the Q-function. Since the occurrence of bit 1 and bit 0 is equal, the overall BER performance is given by

$$\begin{aligned} P(e) = \ & P(I_m = \sqrt{E_b})P(e\,|\,I_m = \sqrt{E_b}) + P(I_m = -\sqrt{E_b})P(e\,|\,I_m = -\sqrt{E_b}) \\ = \ & P(e\,|\,I_m = \sqrt{E_b}) \\ = \ & \sum P(I_{m-1},\ \ldots, I_{m-k})P(e\,|\,I_m = \sqrt{E_b},\ I_{m-1},\ \ldots, I_{m-k}). \end{aligned} \tag{3.25}$$

Due to the ISI from the k preceding bits, BER performance is expected to be reduced significantly without performing equalization on the received signal. Several signal equalization techniques have been developed to mitigate ISI [32]. Here the time domain zero-forcing (ZF) equalization is used to suppress ISI [32, 38]. Let $\{c_n\}$ be the coefficient of the ZF equalizer, and $\{q_n\}$ be the output of the equalizer. Then $\{q_n\}$ is the convolution of $\{c_n\}$ and the channel response h. Ideally, $\{q_n\}$ should be given by

$$q_n = \sum_{m=-\infty}^{\infty} c_m h_{n-m} = \begin{cases} 1 & (n = 0) \\ 0 & (n \neq 0) \end{cases}. \tag{3.26}$$

For a non-ideal equalizer with a finite number of taps, $q_n \neq 0$ when $n \neq 0$, i.e., residual ISI exists. Replacing $h = [1\ a_1 \ldots a_k]$ in Eq. (3.22) with $\{q_n\}$ and substituting y_m into Eq. (3.25), the improved BER performance with time domain ZF equalization is attained.

Figure 3.10 (b) shows the BER performance of both the theoretical analysis and Monte-Carlo (MC) simulation with and without ZF equalization. The theoretical results agree with the simulation results very well (they are completely overlapped in the figure); the BER performance is significantly improved after applying ZF equalization. As an example, the required total LED power is 6.2 W for achieving a BER of 5×10^{-4} without ZF equalization, while the required total LED power is reduced to 3.0 W with ZF equalization. Thus ZF equalization provides 3.2 dB improvement in power reduction. It is also observed that the BER performance with ZF equalization is almost the same as

that without ISI (the two curves are completely overlapped). This means that the ISI can be totally mitigated by ZF equalization. By applying an FEC code, error-free transmission could be attained under this BER requirement [34].

3.3.3 Channel capacity analysis

For a noisy communication channel, the channel capacity is defined as the maximum mutual information between the input and output of the channel over the input distribution [38]. For a discrete-input and continuous-output VLC channel, the channel capacity can be expressed by

$$\begin{aligned} C &= \max_{P_X(\cdot)} I\,(X;Y) \\ &= \max_{P_X(\cdot)} \sum_{x\in X} P_X(x) \int_{-\infty}^{\infty} f_{Y|X}(y\,|\,x) \log_2 \frac{f_{Y|X}(y\,|\,x)}{f_Y(y)}\,dy, \end{aligned} \tag{3.27}$$

where $P_X(.)$ is the input distribution, x is the discrete-input symbol in the set of X, $f_Y(y)$ is the probability density function of the continuous-output signal y, and $f_{Y|X}(y|x)$ is the conditional probability density function of y when the given input symbol is x. Assuming that the input-discrete signal is a bipolar OOK signal, $f_{Y|X}(y|x)$ is given by,

$$\begin{cases} f_{Y|X}(y\,|\,x=-1) = \dfrac{1}{\sqrt{2\pi}\sigma_N} \exp\left(-\dfrac{(y+1)^2}{2\sigma_N^2}\right), \\ f_{Y|X}(y\,|\,x=+1) = \dfrac{1}{\sqrt{2\pi}\sigma_N} \exp\left(-\dfrac{(y-1)^2}{2\sigma_N^2}\right), \end{cases} \tag{3.28}$$

where σ_N^2 is the variance of noise. Considering the ISI discussed in Section 3.3.2, the conditional probability density function in Eq. (3.28) can be expressed by

$$\begin{aligned} & f_{Y|X}(y_m\,|\,x_m) \\ &= \sum p(x_{m-1},\ \ldots, x_{m-k}) f_{Y|X}(y_m\,|\,x_m,\ x_{m-1},\ \ldots, x_{m-k}) \\ &= \sum \frac{p(x_{m-1},\ \ldots, x_{m-k})}{\sqrt{2\pi}\sigma_N} \exp\left(-\frac{\left(y - [x_m,\ x_{m-1},\ \ldots, x_{m-k}][1,\ a_1,\ \ldots,\ a_k]'\right)^2}{2\sigma_N^2}\right), \end{aligned} \tag{3.29}$$

where $h = [1\ a_1\ \ldots\ a_k]$ is the channel response, x_m is the present transmitted bit and $x_{m-1},\ldots,x_{m-k}$ are the k previous transmitted bits. Substituting Eq. (3.29) into Eq. (3.27), the channel capacity of a bipolar OOK signal with ISI in a VLC system can be calculated.

Figure 3.11 shows the calculated channel capacity of a 100 Mbit/s bipolar OOK signal versus total LED lamp power under the arrangement of 12 circle-LED lamps and 4 corner-LED lamps with and without ZF equalization. As shown in Fig. 3.11, the ZF equalization improves the channel capacity significantly. The maximum channel capacity improvement by ZF equalization is 0.17 bits/symbol, which occurs at the total LED power of 2 W. It is also shown in the figure that with ZF equalization, the channel

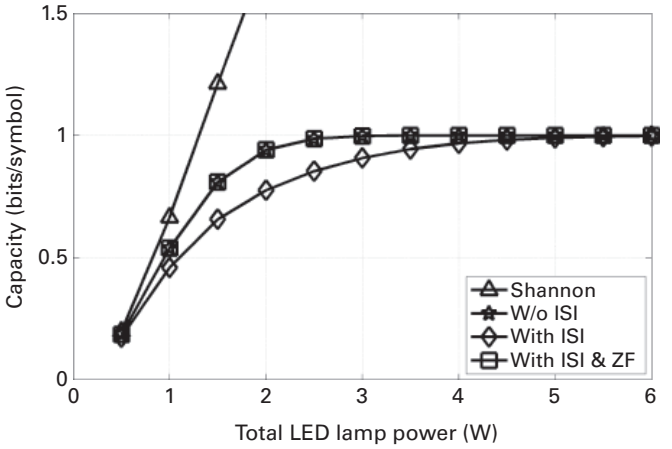

Figure 3.11 Channel capacity of a 100 Mbit/s bipolar OOK signal under the arrangement of 12 circle-LED lamps and 4 corner-LED lamps (adapted from [22]).

capacity remains almost the same as that of the channel without ISI. As a reference, the Shannon capacity is also depicted in Fig. 3.11.

3.4 Dimming control technique and its performance in VLC systems

Illumination and communication are the two major functions of the LED lamps in VLC systems. The brightness of the LED light needs to be adjusted in accordance with the requirements and comfort of users. In addition, adjusting the brightness of LED lamps helps save energy [39]. Pulse width modulation (PWM) is widely used as a dimming control technique [39, 40], where the brightness of the LED light is changed by adjusting the duty cycle of the PWM signal without varying the LED current [20].

As shown in Fig. 3.12 (a), the LED current is modulated by a PWM signal to control its brightness by changing the *on* duration within the whole period. So the light is dimming during the whole period of the PWM signal. The data are modulated onto the dimming-controlled light in the *on* time only, and no light is transmitted during the *off* time as depicted in Fig. 3.12 (b). Since the LED current remains constant throughout, the brightness of the LED light is varied by applying the PWM dimming control signal to adjust the duration of its *on* period as a fraction of the whole period.

With the duty cycle of the PWM signal set to 1, all the LED light is transmitted and the light obtained is of the highest brightness. When the duty cycle is reduced, the LED light in the *off* period is blocked and hence the light is dimming during the whole duration of the PWM signal. It is worth mentioning that the frequency of the PWM signal should be reasonably high, say higher than 200 Hz [41], otherwise it will cause flicker and would have adverse effects on user health [42].

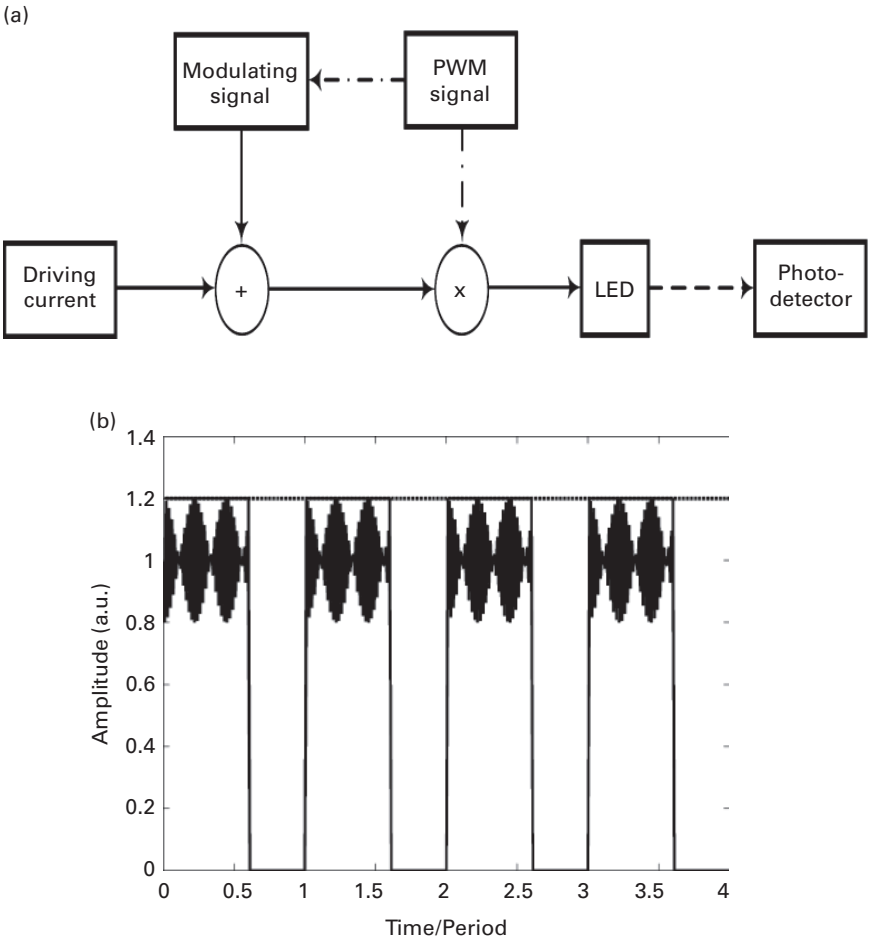

Figure 3.12 (a) Dimming control; (b) signal waveform with dimming control, duty cycle = 0.6 (adapted from [20]).

3.4.1 Bipolar OOK signal under dimming control

As discussed above, with the dimming control, the duration of data transmission in one PWM dimming control signal period (T) is reduced, compared with the case without dimming control. Although the BER performance in the *on* period of the PWM dimming control signal is not changed for a given modulation format, the number of transmitted bits would be reduced in the whole PWM period, which in fact reduces the average data rate. To deal with this problem, the data rate should be increased accordingly while the LED light is dimming, so that the number of transmitted bits remains unchanged. That is, the following equation should hold:

$$R_1 TD = R_0 T, \tag{3.30}$$

where R represents the bit rate of a bipolar OOK signal, and D denotes the duty cycle of a PWM dimming control signal. The subscripts "0" and "1" in Eq. (3.30) correspond to the situations without and with dimming control, respectively. The adaptive data rate under dimming control is shown in Fig. 3.13 (a). In the following analysis, the original data rate R_0 of an OOK signal is assumed to be 10 Mbit/s without dimming control. As depicted in Fig. 3.13 (a), under the dimming control, the adaptive data rate is inversely-proportional

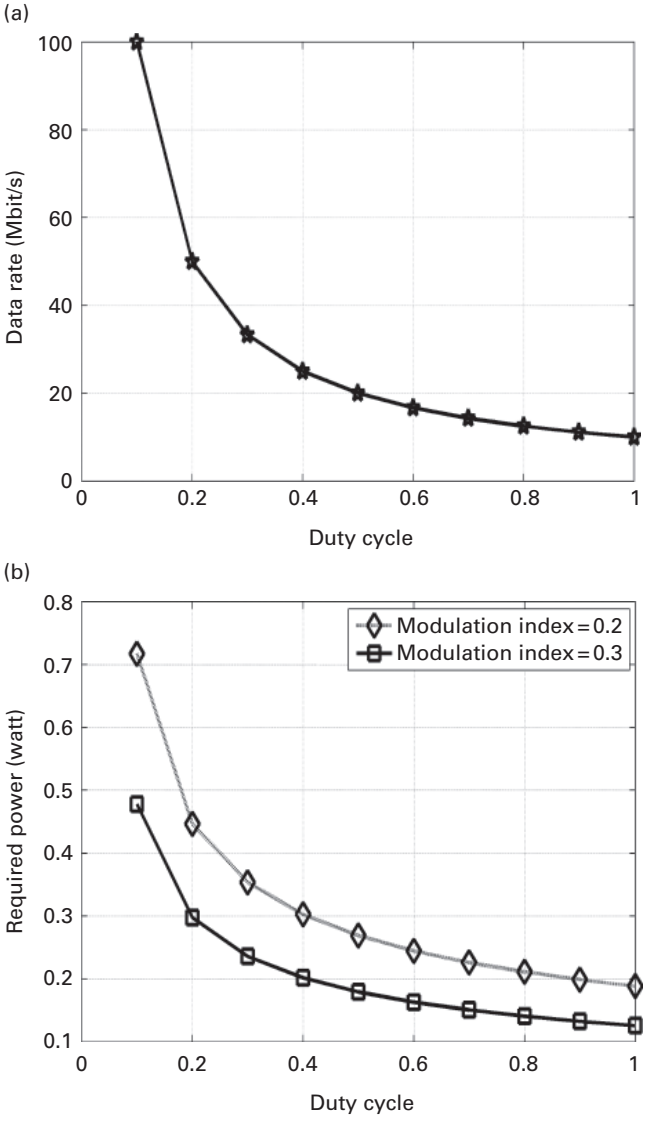

Figure 3.13 (a) Adaptive data rate versus the duty cycle; (b) the required LED lamp power to achieve BER of 10^{-3} without applying dimming control in an OOK VLC system versus the duty cycle (adapted from [20]).

to the duty cycle of the PWM dimming control signal in order to make the number of transmitted bits unchanged. Hence, the adaptive data rate R_1 is higher than the original data rate R_0 and is increased as the duty cycle is reduced. For example, when the duty cycle is 0.1, the adaptive data rate would be 10 times as high as the original data rate, which would make the system hard to implement on the original circuit [20].

Following [43], the BER performance of a bipolar OOK signal is given by

$$BER = Q(\sqrt{2SNR}), \tag{3.31}$$

where $Q(\cdot)$ is the Q-function. As described above, the signal power is kept constant while changing duty cycle; however, the noise power is increased as the data rate grows [1] when the duty cycle decreases, which reduces the BER performance in terms of SNR as shown in Eq. (3.31). Under the dimming control, the BER of less than 10^{-3} should be guaranteed to achieve error-free transmission by applying the FEC code [34]. Substituting Eq. (3.7) into Eq. (3.31), we have

$$BER = Q(\sqrt{2SNR}) = Q\left(\frac{\sqrt{2}RH(0)P_tM_I}{\sigma(P_t)}\right). \tag{3.32}$$

Note that the average power $\overline{f(t)^2}$ of the bipolar OOK signal in Eq. (3.7) is unity and the noise variance σ^2 is related to the total received optical power P_r in terms of the LED lamp power P_t. By solving Eq. (3.32), the required LED lamp power to achieve a BER of 10^{-3} without applying dimming control can be obtained, which is associated with both modulation index M_I and the noise variance, when the locations of LED lamp and receiver are fixed.

In the following scenario, the locations of an LED lamp and receiver are assumed to be [2.5 m, 2.5 m, 3.0 m] and [3.75 m, 1.25 m, 0.85 m], respectively. In addition, the illuminance is assumed to be proportional to the LED's driving current. It is noted that the required LED lamp power to achieve a BER of 10^{-3} should be kept unchanged under the dimming control as well [20]. Figure 3.13 (b) shows the required LED lamp power to achieve a BER of 10^{-3} without applying dimming control versus the duty cycle. When the duty cycle is varied from 1 to 0.3, i.e., the illuminance of LED light is reduced to 30% of the initial illuminance, the required LED lamp powers without applying dimming control increase slowly to 0.35 W and 0.24 W for modulation indices of 0.2 and 0.3, respectively. However, as the duty cycle is further reduced from 0.3 to 0.1, i.e., the illuminance of the LED light is only 10% of the initial illuminance, the required LED lamp power without applying dimming control grows drastically from 0.35 W to 0.72 W when the modulation index is 0.2 and grows from 0.24 W to 0.48 W when the modulation index is 0.3. Since the LED lamp power has to be kept constant throughout the dimming control scheme, in order to achieve a BER of 10^{-3} for the entire duty cycle range of 0.1 to 1, the required LED lamp power should be set as high as 0.72 W if the modulation index is 0.2, and 0.48 W if the modulation index is 0.3. In this way, while the dimming control is applied, the LED lamp power is maintained constant and both average data rate and the BER of 10^{-3} can be guaranteed. The above results reveal that in an OOK VLC system with dimming control, not only the data rate but also the lamp power need to be increased

significantly in order to provide a guarantee of communication quality in terms of BER and average data rate for the entire duty cycle range of 0.1 to 1.

3.4.2 Adaptive M-QAM OFDM signal under dimming control

This subsection analyzes and discusses the performance of an adaptive M-QAM OFDM signal under the dimming control scheme, where M represents the number of points in the signal constellation [44]. Since one symbol of the M-QAM signal carries $\log_2(M)$ bits, the total number of transmitted bits could be kept the same by increasing the symbol rate and/or the value of M when higher level M-QAM is used. Let M_0 be the initial number of points in the signal constellation, and M_1 be the adaptive number of points in the signal constellation. Hence, we have

$$\log_2(M_1)R_1TD = \log_2(M_0)R_0T,$$
$$R_1 = \frac{\log_2(M_0)R_0}{\log_2(M_1)D}, \tag{3.33}$$

where R_0 is the original symbol rate of the M-QAM signal without dimming control, and R_1 is the adaptive symbol rate of the M-QAM signal with dimming control. Here R_0 is assumed to be 10 Msymbol/s. Substituting SNR per symbol in Eq. (3.8) into Eq. (3.16), the BER performance of an M-QAM signal without applying dimming control is obtained from,

$$BER \approx \frac{4}{\log_2(M)}\left(1 - \frac{1}{\sqrt{M}}\right)Q\left(\sqrt{\frac{3}{M-1}\frac{\left(RH(0)P_tM_I\right)^2}{\sigma^2(P_t)}}\right). \tag{3.34}$$

The average power $\overline{f(t)^2}$ of the M-QAM signal in Eq. (3.8) is also unity. Solving Eq. (3.34), the required LED lamp power to achieve a BER of 10^{-3} without applying dimming control of the M-QAM signal is obtained. Note that when OFDM is applied in a VLC system, the bandwidth should be at least twice as large as the symbol rate, due to the application of Hermitian symmetry. In addition, Eqs. (3.16) and (3.34) are the BER performance for an M-QAM with a square constellation. For an M-QAM with non-square constellation, the threshold of SNR per symbol to achieve a BER of 10^{-3} is obtained by using MC simulation.

Based on Eqs. (3.33) and (3.34), the values of R_1 and M_1 under different duty cycles can be calculated. Table 3.5 shows the relationship between M_1 and the duty cycle for adaptive M-QAM with dimming control. As expected, the value of M_1 increases as the duty cycle is reduced. Figure 3.14 (a) shows the relationship between the adaptive

Table 3.5 Relationship between M_1 and duty cycle for adaptive M-QAM with dimming control.

Duty cycle	0.1	0.2	0.3	0.4	0.5	0.6	0.7	0.8	0.9	1.0
M_1	256	128	64	32	16	16	8	8	8	4

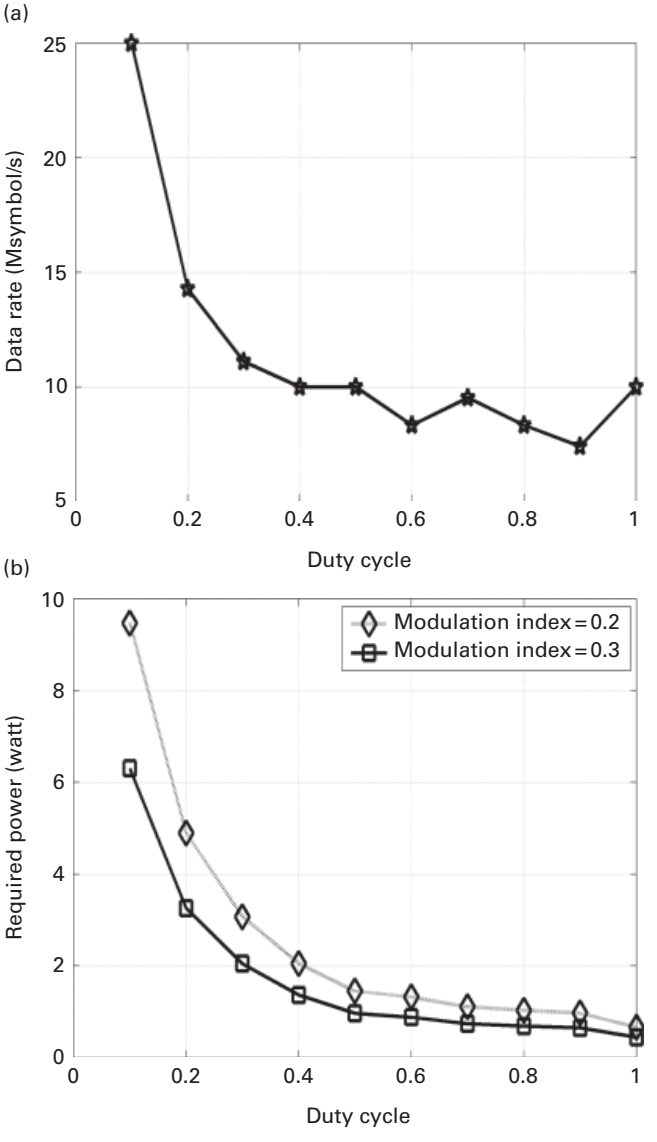

Figure 3.14 (a) Adaptive symbol rate of M-QAM signal versus the duty cycle; (b) the required LED lamp power to achieve BER of 10^{-3} without applying dimming control versus the duty cycle.

symbol rate R_1 and the duty cycle. When the duty cycle is less than 0.3, the adaptive symbol rate has to increase significantly to satisfy the communication quality. The highest adaptive rate is 2.5 times as high as the original symbol rate when the duty cycle is 0.1, which is the same as that of an OOK signal when the duty cycle is 0.4, as shown in Fig. 3.13 (a). Hence, the increase in the symbol rate of an M-QAM OFDM signal is moderate compared with that of an OOK signal.

Figure 3.14 (b) shows the relationship between the required LED lamp power and the duty cycle. When the duty cycle is greater than 0.4, the required LED lamp power increases slowly as the duty cycle decreases. When the duty cycle is 0.9, the required LED lamp powers without applying dimming control are 0.97 W and 0.65 W for the modulation indices of 0.2 and 0.3, respectively, which are larger than the required LED lamp power of an OOK signal with a 0.1 duty cycle. However, the required LED lamp power increases rapidly when the duty cycle is reduced below 0.4. When the duty cycle is 0.1, the required LED lamp powers of *M*-QAM OFDM signals are 9.5 W and 6.3 W for the 0.2 and 0.3 modulation indices, respectively, which are more than 13 times larger than the corresponding required LED lamp powers of an OOK signal. Hence, when the duty cycle is larger than 0.4, the adaptive *M*-QAM OFDM signal remains to be a good choice to be incorporated with a dimming control scheme, since the required LED lamp power without applying dimming control is about 2 W and the adaptive symbol rate is not larger than the original symbol rate.

3.5 Summary

This chapter describes three recently developed approaches to improve the performance of visible light communication systems. Section 3.2 discusses a receiver plane tilting technique to reduce the SNR fluctuation in a room. This scheme can provide 5.69 dB and 4.14 dB improvement for the peak-to-trough SNR performance, for the cases of one LED lamp and four LED lamps, respectively. The corresponding maximum spectral efficiency improvements are 0.47 bit/s/Hz and 0.23 bit/s/Hz, respectively. Section 3.3 describes an LED lamp arrangement technique to improve SNR and BER performances. It is shown that the arrangement of 12 LED lamps in a circle and 4 LED lamps at corners can attain much better performance than other possible arrangements. By applying the time domain zero-forcing equalization, this LED lamp arrangement is able to provide almost identical communication qualities in terms of SNR and BER to all users at different positions throughout the room. In Section 3.4, the performance of a VLC system under a dimming control scheme is discussed for two different modulation formats, namely OOK and *M*-QAM OFDM. The results show that the adaptive data rate of an OOK signal is always larger than the original data rate, while the required LED lamp power is less than 1 W, when the original data rate is 10 Mbit/s. The adaptive data rate of the *M*-QAM OFDM signal is not larger than the original symbol rate when the duty cycle is larger than 0.4, however, the LED lamp required without applying dimming control is always larger than that required by the OOK signal.

References

[1] T. Komine and M. Nakagawa, "Fundamental analysis for visible-light communication system using LED lights," *IEEE Transactions on Consumer Electronics*, **50**, 100–107, 2004.

[2] D. C. O'Brien, G. Faulkner, K. Jim, *et al*., "High-speed integrated transceivers for optical wireless," *IEEE Communications Magazine*, **41**, 58–62, 2003.
[3] J. Vucic, C. Kottke, K. Habel, and K. D. Langer, "803 Mbit/s visible light WDM link based on DMT modulation of a single RGB LED luminary," in *Optical Fiber Communication/*National Fiber Optic Engineers Conference (OFC/NFOEC), 2011, pp. 1–3.
[4] H. Elgala, R. Mesleh, and H. Haas, "Indoor broadcasting via white LEDs and OFDM," *IEEE Transactions on Consumer Electronics*, **55**, 1127–1134, 2009.
[5] J. M. Kahn and J. R. Barry, "Wireless infrared communications," *IEEE Proceedings*, **85**, 265–298, 1997.
[6] K. D. Langer and J. Grubor, "Recent developments in optical wireless communications using infrared and visible light," in International Conference on *Transparent Optical Networks (ICTON)*, 2007, pp. 146–151.
[7] S. Hann, J.-H. Kim, S.-Y. Jung, and C.-S. Park, "White LED ceiling lights positioning systems for optical wireless indoor applications," in European Conference and Exhibition on *Optical Communication (ECOC)*, 2010, pp. 1–3.
[8] L. Zeng, D. O'Brien, L.-M. Hoa, *et al*., "Improvement of data rate by using equalization in an indoor visible light communication system," in International Conference on *Circuits and Systems for Communications (ICCSC)*, 2008, pp. 678–682.
[9] G. Ntogari, T. Kamalakis, and T. Sphicopoulos, "Performance analysis of space time block coding techniques for indoor optical wireless systems," *IEEE Journal on Selected Areas in Communications*, **27**, 1545–1552, 2009.
[10] D. Bykhovsky and S. Arnon, "An experimental comparison of different bit-and-power-allocation algorithms for DCO-OFDM," *Journal of Lightwave Technology*, **32**, 1559–1564, 2014.
[11] D. Bykhovsky and S. Arnon, "Multiple access resource allocation in visible light communication systems," *Journal of Lightwave Technology*, **32**, 1594–1600, 2014.
[12] G. Cossu, A. M. Khalid, P. Choudhury, R. Corsini, and E. Ciaramella, "3.4 Gbit/s visible optical wireless transmission based on RGB LED," *Optics Express*, **20**, B501–B506, 2012.
[13] D. Tsonev, H. Chun, S. Rajbhandari, *et al*., "A 3-Gb/s single-LED OFDM-based wireless VLC link using a gallium nitride μLED," *IEEE Photonics Technology Letters*, **26**, 637–640, 2014.
[14] T. Fath, M. Di Renzo, and H. Haas, "On the performance of space shift keying for optical wireless communications," in *IEEE GLOBECOM Workshops (GC Wkshps)*, 2010, pp. 990–994.
[15] R. Mesleh, R. Mehmood, H. Elgala, and H. Haas, "Indoor MIMO optical wireless communication using spatial modulation," in IEEE International Conference on *Communications (ICC)*, 2010, pp. 1–5.
[16] R. Mesleh, H. Elgala, and H. Haas, "Optical spatial modulation," *IEEE/OSA Journal of Optical Communications and Networking*, **3**, 234–244, 2011.
[17] T. Fath and H. Haas, "Performance comparison of MIMO techniques for optical wireless communications in indoor environments," *IEEE Transactions on Communications*, **61**, 733–742, 2013.
[18] http://www.ted.com/talks/harald_haas_wireless_data_from_every_light_bulb.html.
[19] J. Chen, C. Yu, Z. Wang, J. Shen, and Y. Li, "Indoor optical wireless integrated with white LED lighting: Perspective & challenge," in 10th International Conference on *Optical Communications and Networks (ICOCN)*, 2011, pp. 1–2.

[20] Z. Wang, W. D. Zhong, C. Yu, *et al*., "Performance of dimming control scheme in visible light communication system," *Optics Express*, **20**, 18861–18868, 2012.
[21] Z. Wang, C. Yu, W. D. Zhong, and J. Chen, "Performance improvement by tilting receiver plane in M-QAM OFDM visible light communications," *Optics Express*, **19**, 13418–13427, 2011.
[22] Z. Wang, C. Yu, W. D. Zhong, J. Chen, and W. Chen, "Performance of a novel LED lamp arrangement to reduce SNR fluctuation for multi-user visible light communication systems," *Optics Express*, **20**, 4564–4573, 2012.
[23] Z. Wang, W. D. Zhong, C. Yu, and J. Chen, "A novel LED arrangement to reduce SNR fluctuation for multi-users in visible light communication systems," in 8th International Conference on *Information, Communications and Signal Processing (ICICS)*, 2011, pp. 1–4.
[24] Z. Wang, C. Yu, W. D. Zhong, J. Chen, and W. Chen, "Performance of variable M-QAM OFDM visible light communication system with dimming control," in 17th *Opto-Electronics and Communications* Conference *(OECC)*, 2012, pp. 741–742.
[25] Z. Wang, J. Chen, W. D. Zhong, C. Yu, and W. Chen, "User-oriented visible light communication system with dimming control scheme," in 11th International Conference on *Optical Communications and Networks (ICOCN)*, 2012, pp. 1–4.
[26] H. Kressel, *Semiconductor Devices for Optical Communication*, Springer-Verlag, 1982.
[27] J. R. Barry, *Wireless Infrared Communications*, Kluwer Academic Publishers, 2006.
[28] I. Neokosmidis, T. Kamalakis, J. W. Walewski, B. Inan, and T. Sphicopoulos, "Impact of nonlinear LED transfer function on discrete multitone modulation: Analytical approach," *IEEE Journal of Lightwave Technology*, **27**, 4970–4978, 2009.
[29] C. H. Edwards and D. E. Penney, *Calculus*, Prentice Hall, 2002.
[30] M. T. Heath, *Scientific Computing – An Introductory Survey*, McGraw-Hill, 2002.
[31] A. Svensson, "An introduction to adaptive QAM modulation schemes for known and predicted channels," *IEEE Proceedings*, **95**, 2322–2336, 2007.
[32] J. Proakis, *Digital Communications*, 3rd ed., McGraw-Hill, 1995.
[33] F. Xiong, *Digital Modulation Techniques*, 2nd ed., Artech House, 2006.
[34] R. J. Essiambre, G. Kramer, P. J. Winzer, G. J. Foschini, and B. Goebel, "Capacity limits of optical fiber networks," *IEEE Journal of Lightwave Technology*, **28**, 662–701, 2010.
[35] M. Z. Afgani, H. Haas, H. Elgala, and D. Knipp, "Visible light communication using OFDM," in International Conference on *Testbeds and Research Infrastructures for the Development of Networks and Communities (TRIDENTCOM)*, 2006, pp. 6–134.
[36] J. Armstrong, "OFDM for optical communications," *IEEE Journal of Lightwave Technology*, **27**, 189–204, 2009.
[37] U. S. Jha and R. Prasad, *OFDM towards Fixed and Mobile Broadband Wireless Access*, Artech House, 2007.
[38] A. Goldsmith, *Wireless Communications*, Cambridge University Press, 2005.
[39] H. Sugiyama, S. Haruyama, and M. Nakagawa, "Brightness control methods for illumination and visible-light communication systems," in 3rd International Conference on *Wireless and Mobile Communications (ICWMC)*, 2007, pp. 78–83.
[40] J.-H. Choi, E.-B. Cho, T.-G. Kang, and C. G. Lee, "Pulse width modulation based signal format for visible light communications," in 15th *Opto-Electronics and Communications* Conference *(OECC)*, 2010, pp. 276–277.
[41] S. Rajagopal, R. D. Roberts, and S.-K. Lim, "IEEE 802.15.7 visible light communication: Modulation schemes and dimming support," *IEEE Communications Magazine*, **50**, 72–82, 2012.

[42] G. Ntogari, T. Kamalakis, J. Walewski, and T. Sphicopoulos, "Combining illumination dimming based on pulse-width modulation with visible-light communications based on discrete multitone," *IEEE/OSA Journal of Optical Communications and Networking*, **3**, 56–65, 2011.

[43] J. Proakis and M. Salehi, *Contemporary Communication Systems Using MATLAB*, PWS Pub., 1998.

[44] A. J. Goldsmith and S.-G. Chua, "Variable-rate variable-power MQAM for fading channels," *IEEE Transactions on Communications*, **45**, 1218–1230, 1997.